# A Digital Nanoplasmonic Microarray Immunosensor for Multiplexed Cytokine Monitoring during CAR T-Cell Therapy from a Leukemia Tumor Microenvironment Model

Benteng Ma<sup>1</sup>, Xinya Liu<sup>1</sup>, Zhuoyu Zhang<sup>2</sup>, Chao Ma<sup>2</sup>, Rashik Chand<sup>3</sup>, Saee Patwardhan<sup>1</sup>, Chuanyu Wang<sup>4</sup>, Soracha D. Thamphiwatana<sup>5</sup>, Pengyu Chen<sup>4</sup>, Weiqiang Chen<sup>\*1,2,6</sup>

<sup>1</sup>Department of Biomedical Engineering, New York University, Brooklyn, NY 11201, USA <sup>2</sup>Department of Mechanical and Aerospace Engineering, New York University, Brooklyn, NY 11201, USA

<sup>3</sup>Division of Engineering, New York University Abu Dhabi, Abu Dhabi, United Arab Emirates
 <sup>4</sup>Department of Material Engineering, Auburn University, Auburn, AL 36849, USA
 <sup>5</sup>Department of Biomedical Engineering, Faculty of Engineering, Mahidol University, Nakorn
 Pathom 73170, Thailand

<sup>6</sup>Perlmutter Cancer Center, NYU Langone Health, New York, NY 10016, USA

\*Correspondence should be addressed to W. Chen (email: wchen@nyu.edu)

Departments of Biomedical Engineering, Mechanical and Aerospace Engineering, New York

University, Brooklyn, NY 11201, USA

Keywords: Biosensor, Cytokine, Organ-on-a-chip, Leukemia, CAR T-cell therapy

# **Abstract**

The release of cytokines by chimeric antigen receptor (CAR) T-cells and tumor resident immune cells defines a significant part of CAR T-cell functional activity and patient immune responses during CAR T-cell therapy. However, few studies have so far precisely characterized the cytokine secretion dynamics in the tumor niche during CAR T-cell therapy, which requires multiplexed, and timely biosensing platforms and integration with biomimetic tumor microenvironment. Herein, we implemented a digital nanoplasmonic microarray immunosensor with a microfluidic biomimetic Leukemia-on-a-Chip model to monitor cytokine secretion dynamics during CD19 CAR T-cell therapy against precursor B-cell acute lymphocytic leukemia (B-ALL). The integrated nanoplasmonic biosensors achieved precise multiplexed cytokine measurements with low operating sample volume, short assay time, heightened sensitivity, and negligible sensor crosstalk. Using the digital nanoplasmonic biosensing approach, we measured the concentrations of six cytokines (TNF-α, IFN-γ, MCP-1, GM-CSF, IL-1β, and IL-6) during first 5 days of CAR T-cell treatment in the microfluidic Leukemia-on-a-Chip model. Our results revealed a heterogeneous secretion profile of various cytokines during CAR T-cell therapy and confirmed a correlation between the cytokine secretion profile and the CAR T-cell cytotoxic activity. The capability to monitor immune cell cytokine secretion dynamics in a biomimetic tumor microenvironment could further help in study of cytokine release syndrome during CAR T-cell therapy and in development of more efficient and safer immunotherapies.

#### 1. Introduction

Chimeric antigen receptor (CAR) T-cell therapy has recently emerged has a novel treatment against cancer (Wang, Wu et al. 2017). Anti-CD19 CAR T-cell therapy, arguably the most successful CAR T-cell therapy to date in the clinic, involves genetically engineering autologous T-cells ex vivo to express CARs against a B-lineage antigen CD19, which is expressed on tumor cells such as diffuse large B-cell lymphoma and precursor B-cell acute lymphocytic leukemia (B-ALL) (Sadelain 2017). Upon reorganization of tumor antigen by CAR, a wave of signals that comprise the secretion of cytolytic enzymes, stimulatory cytokines, and chemoattractive proteins is inflicted in CAR T-cells (Bonifant, Jackson et al. 2016). The profile of cytokine release by CAR T-cells, as well as tumor resident immune cells, defines a significant part of their functional activity, which is significantly associated with patient immune responses (Alizadeh, Wong et al. 2021). However, how the time evolution of patient cytokine secretion and cytokine-mediated CAR T-cell cross-talk with the tumor microenvironment associated with clinical outcomes remains unclear, and this is further compounded by immunotoxic side effects such as cytokine release syndrome (CRS) commonly seen during the CAR T-cell therapy (Brudno and Kochenderfer 2019). Moreover, this CRS response, which varies between patients and differs in CAR design, is difficult to predict, highlighting a pressing need to systematically evaluate the cytokine secretion dynamics and to link this capability to clinical outcomes.

Current methods for cytokine measurement are flow cytometry, intracytoplasmic cytokine staining (ICS), enzyme-linked immunosorbent assay (ELISA), and enzyme-linked immunospot (ELISpot) assay (Taguchi, McGhee et al. 1990, Prussin and Metcalfe 1995, Freer and Rindi 2013, Aydin 2015). These methods do provide valuable information for cytokine analysis, but they have several shortcomings, for instance, flow cytometry for detection of cytokines accumulated inside cells requires fixation and permeabilization. Such a technical treatment prohibits time-course experiments or post-detection of processed cells (Vignali 2000). Recently, some alternative platforms are being developed including bead ELISA systems like Simoa (Mora, Given Chunyk et al. 2014) and pEdELISA (Song, Sandford et al. 2021), or microbalance (Chen, Huang et al. 2015, Lim, Saha et al. 2020). Yet, these systems mostly achieved multiplexed detection of cytokines in one sample using fluorescence which is limited by the separation of dye channels. Localized surface plasmon resonance (LSPR) based nanoplasmonic biosensors have recently shown great potential for rapid and high-sensitivity biomolecule sensing (Mayer and Hafner 2011).

Early efforts for LSPR biosensing development were mainly focused on identifying the optimum nanoparticle configuration for maximum detection sensitivity, yet systematic investigation of their performance in real-life applications is limited, which requires an advanced liquid sample handling interface compatible with the peculiarity of the detection principle. Furthermore, the inability to simultaneously achieve high sensitivity, specificity, and multiplexing of current plasmonic technique prohibits its use for accurate, high-throughput, multifunctional immune analysis, hindering the translation of this technique towards practical biomarker detection in complex clinical samples. Recently, we have proposed a novel digital nanoplasmonic immunoassay method to use large-size nanoparticles to detect cytokines, where these particles have intense scattering and allows digital counting of single particle from images taken by darkfield microscopy (Gao, Song et al. 2021). Our nanoplasmonic biosensing approach is suitable yet need to be optimized for implementation on highly functional biochip system such as organ-on-a-chip for cancer immunotherapy study, which requires sensitive, multiplex and time-course measurement of cytokine secretions with a small sample volume that conventional assays like ELISA can hardly address these requirements.

In this study, we developed a novel digital nanoplasmonic microarray immunosensor to monitor cytokine secretion dynamics during anti-CD19 CAR T-cell therapy against B-ALL for a microfluidic Leukemia-on-a-Chip model. The cytokine detection followed a simple immunoassay and digital imaging readout with a single analyte resolution. The digital nanoplasmonic microarray immunosensor achieved precise multiplexed cytokine measurements with low operating sample volume, short assay time, heightened sensitivity, and negligible sensor crosstalk. As a proof-of-concept application, we monitored the profile of cytokine secretion from the microfluidic leukemia tumor microenvironment model during CAR T-cell therapy. Our results revealed a heterogeneous secretion of various cytokines from CAR T-cell therapy, which correlated to CAR T-cell cytotoxic activity. Taken together, we believe future on-chip integration can realize *in-situ* and real-time monitoring of cytokine secretion dynamics in a biomimetic tumor microenvironment, which can help to elucidate the mechanisms contributed by interactions between multiple immune cell populations underlying CRS during CAR T-cell therapy.

#### 2. Materials and Methods

#### 2.1. Microfabrication of microfluidic channels

Polydimethylsiloxane (PDMS) slabs with microfluidic channels were prepared with a standard soft lithography approach (Ma, Witkowski et al. 2020). In brief, master molds of microfluidic channels were fabricated by photolithographic patterning 50 µm thick SU-8 photoresist (Kayaku SU-8 2050) on a silicon wafer. Master molds were plasma treated and then salinized with trichloro(1*H*,1*H*,2*H*,2*H*-perfluorooctyl)silane (Sigma Aldrich) overnight in a vacuum desiccator to facilitate later peeling off the PDMS from the molds. After preparing the mast molds, PDMS (Sylgard 184, Corning) elastomer and curing agent was prepared at a mass ratio of 10:1 and poured onto the molds. After thorough degassing, the PDMS precursor was cured at 80°C for 6 hours. Cured PDMS slabs were then peeled off from the molds, cut into small pieces, punched with biopsy perforator (Electronic Microscopy System) to generate inlets and outlets, and stored for future use.

## 2.2. Preparation of capture antibody microarrays

Glass slides (Corning) were first cleaned with piranha solution (3:1 mixture of sulfuric acid (H<sub>2</sub>SO<sub>4</sub>, Sigma Aldrich) and 30% hydrogen peroxide (H<sub>2</sub>O<sub>2</sub>, Sigma Aldrich)) for 15 minutes, rinsed with deionized water (Milli Q) thoroughly, and ultrasonicated in an ultrasonic bath (Thermo Fisher Scientific) in water for 20 minutes to activate the surface of glass slides. Cleaned and activated glass slides were immersed in a freshly prepared 2% (3-Aminopropyl)triethoxysilane (APTES, Sigma Aldrich) aqueous solution for 1 hour, after which the slides were rinsed with deionized water thoroughly and baked at 110°C for at least 2 hours. The as-prepared APTES functionalized glass slides were reversibly assembled with PDMS slabs with microfluidic patterning channels. The microfluidic channels were then filled with 5% glutaraldehyde aqueous solution (diluted from 50% solution, Thermo Fisher Scientific), and incubated at room temperature overnight to facilitate antibody engraftment. Following a thorough rinse with deionized water, 10 µL 100 µg/mL capture antibody solutions of TNF-α, IFN-γ, MCP-1, GM-CSF, IL-1b, and IL-6 (BioLegend) in phosphate buffered saline (PBS, Sigma Aldrich) as well as 5 µg/mL APC-labeled mouse IgG1 isotype control solution (BioLegend) in PBS were filled into corresponding microfluidic channels and incubated at 4°C overnight. After incubation, the channels were washed with PBS, incubated with a 200 mM glycine (Sigma Aldrich) and 10 mM sodium borohydride (Sigma Aldrich) solution in PBS for 1

hour to deactivate remaining glutaraldehyde. Then the channels were blocked with 2% bovine serum albumin (BSA, Biolegend) in a PBST buffer (PBS with 0.05% Tween-20 (Sigma Aldrich)) for 1 hour, followed by a thorough wash with PBST. The prepared chips were then stored at 4 °C and used within 5 days. Subsequently, the PDMS channel slabs were removed and the glass slides were immersed in PBST, then in PBS with 1 M sodium chloride (Sigma Aldrich) solution to mitigate possible antibody denaturation due to water immersion, followed by dipped in deionized water for 10 times, and air blown to dry. Finally, a second PDMS slab with microfluidic sample-flow channels for sample loading was reversibly bonded to the glass slide, with 2% BSA, 5% sucrose (Sigma Aldrich), and 0.02% sodium azide (Sigma Aldrich) in PBST filled in the channels and were stored at 4°C before use.

#### 2.3. Preparation of streptavidin-conjugated gold nanoparticles.

Lipoic acid coated gold nanoparticles (AuNPs, 100 nm, Nanocomposix) have -COOH group on their surfaces. **EDC/NHS** (N-ethyl-N'-(3-(dimethylamino)propyl)carbodiimide/Nhydroxysuccinimide) reaction was used for conjugation of streptavidin on the particles. Briefly, 100 μL 1 mg/mL lipoic acid coated AuNP solution was diluted to 500 μL with deionized water and was mixed with 4 µL freshly prepared 10 mg/mL EDC (Thermo Fisher Scientific) and 8 µL freshly prepared 10 mg/mL sulfo-NHS (Thermo Fisher Scientific). The solution was shaken for 30 minutes and then centrifuged (400 g, 10 min). The supernatant was removed and 500 µL 5 mM sodium phosphate buffer (pH 7.4) with 0.5% Poly(ethylene glycol) PEG-22k (provided in Nanocomposix High Sensitivity Gold Conjugation Kit GSZR150-10M) was added to redisperse the pellet, and the solution was ultrasonicated for 10 seconds for thorough redispersion. The solution was centrifuged again, and the supernatant was replaced by 200 µL 5 mM carbonate buffer (pH 9.6, formulated by sodium bicarbonate and sodium carbonate, Sigma Aldrich) with 0.5% PEG-35k (Sigma Aldrich). Following this, AuNPs were pelleted and redispersed by ultrasonication, and reacted with 2 µL 10 mg/mL streptavidin (VWR) in water for 3 hours under shaking. Afterward, 2 µL 50% hydroxylamine (Thermo Fisher Scientific) was added to the solution to quench any remaining sulfo-NHS intermediate product. After shaking for 10 minutes, the solution was washed by centrifugation, replacement of buffer, and ultrasonication for redispersion two times with carbonate buffer. After the final centrifugation, the supernatant was replaced by 200 µL 1% BSA, 1% Tween-20, 0.02% sodium azide in PBST, then redispersed by

ultrasonication, and shaken for 1 hour for blocking. The streptavidin-conjugated AuNP solution was then stored at 4°C and would be diluted with 1% BSA in PBST to 1/4 concentration before use.

#### 2.4. Detection of cytokines by the nanoplasmonic immunoassay

Before loading, a sample solution was mixed at a 1:1 volume ratio with a detection antibody cocktail containing 1 μg/mL TNF-α, IFN-γ, IL-1b, IL-6 (Invitrogen) and 1.25 μg/mL MCP-1, GM-CSF (BioLegend) biotin-conjugated detection antibodies. Mixture of 3 µL sample and 3 µL detection antibody cocktail was injected into each microfluidic sample-flow channel using a micropipette. After on-chip capture of target cytokine molecules, the channels were thoroughly washed with PBST and incubated with filled with the streptavidin-conjugated AuNP solution for 1 hour. The AuNP solution was washed out by PBST, and the device was then dismantled, and the glass slide was dipped into deionized water and air-dried. Following this, the glass slide was mounted on a 3D printed homemade specimen holder on a Zeiss Imager.M2 microscope with a darkfield condenser. An in-house program was developed to control the microscope to scan the microarrays, and the bright dots of immobilized AuNPs were imaged with a 40x, 0.45 NA objective lens, with 43HE filter set to reduce noise. The images were collected and analyzed by customized protocol with ImageJ (NIH) software, where the bright dots were segmented based on local maxima with contrast to vicinity (prominence) of 1500, and the counted number was used for measurement of the concentration following a calibration curve formed by a series of known concentration gradients and fitted to a linear curve of concentration to bright spot number.

# 2.5 Preparation of Leukemia-on-a-chip for CAR T-cell therapy study

The preparation of leukemia-on-a-chip was adopted from our previous work (Ma, Witkowski et al. 2020, Witkowski, Dolgalev et al. 2020) with slight modifications. Briefly, different compartments of the microfluidic device were sequentially infused with cell-containing hydrogel solutions by mixing 3  $\mu$ L freshly prepared 6 mg/mL fibrinogen (Sigma Aldrich) in PBS and 3  $\mu$ L cell suspension with calculated cell numbers with 2U/mL thrombin (Sigma Aldrich). The cell suspension for the inner ring included human umbilical vein endothelial cells (HUVECs,  $3\times10^7$  cells/mL, Lonza) and B-ALL (Reh,  $5\times10^6$  cells/mL, ATCC), while the peripheral ring included

normal human lung fibroblasts (3×10<sup>6</sup> cells/mL, Lonza) and macrophages (2.5×10<sup>6</sup> cells/mL). Macrophages were derived from THP-1 monocytes (ATCC) with 100 ng/mL phorbol-12myristate-13-acetate (PMA, Sigma Aldrich) for 24 hours. After cell loading, the system was cultivated for 5 days to establish microvasculature with medium of 50% EGM-2 (Lonza) and 50% RPMI-1640 (10% fetal bovine serum, Themo Fisher Scientific). To characterize the resultant chip, vascular cells were stained with FITC anti-human CD31 (BioLegend), Reh leukemia blasts were stained with PE anti-human CD19 (BioLegend), and macrophages were stained with APC antihuman CD68 (BioLegend), respectively, then the immuno-stained leukemia devices were then imaged with a Nikon C2i confocal microscope. Following the establishment of leukemia-on-achip, anti-CD19 4-1BB $\delta$  CAR T-cells (ProMab) at different dosages  $(0, 5 \times 10^3, \text{ and } 2.5 \times 10^4 \text{ cells},$ referred as to 0, 5k, and 25k groups, respectively) were infused into the central hole of the device and diffused into the microvasculature. CAR T-cells then infiltrated into the leukemia niche and killed leukemia cells. To clearly visualize and distinguish CAR T-cell and leukemia blasts, 4-1BBζ CAR T-cells were pre-labeled with Vybrant DiD Cell-Labeling Solution (Thermo Fischer Scientific), whereby Reh leukemia blasts were genetically engineered to express with GFP. To quantify the leukemia burden after on-chip infusion of CAR T-cells, the leukemia chips were imaged under an inverted microscope (Zeiss Axio Observer.Z1) with a 20× objective every 24 hours. The count of live leukemia cells (presence of GFP signal) from individual 20× field view images were used for a quantification of leukemia burden on-chip treated with CAR T-cells at different dosages (0, 5k, and 25k) on each day. Cell culture media was collected every 24 hours for 5 days from the devices for later cytokine detections and fresh media was added subsequently onto the devices. Cytokine concentrations of each CAR T-cell dosage condition were measured from three independent experiments. The sample for each independent experiment was collected and mixed from two repeating devices to reduce random errors.

#### 2.6 Statistics

All statistical analysis was performed by Tukey test on one-way analysis of variance (ANOVA) using OriginPro2022b (OriginLab). \*P < 0.05 and \*\*P < 0.01 were considered significantly different. The results, including the error bars in the graphs, were given as means  $\pm$  standard derivations (SD). Details are reported in each figure.

#### 3. Results and Discussion

## 3.1. Nanoplasmonic microarray immunosensor for cytokine detection

The nanoplasmonic microarray immunosensor for cytokine detection combines digital nanoplasmonic imaging technology with a simple sandwich immunoassay (**Figure 1**). In principle, different cytokine capture antibodies (CAbs) were first patterned onto a standard microscope glass slide (**Figure 1A**) and employed to capture and immobilize target cytokine antigens (TNF-α, IFN-γ, MCP-1, GM-CSF, IL-1β, and IL-6) from introduced biological samples. Then, plasmonic AuNPs (100 nm nanospheres) functionalized with matching detection antibodies (DAbs) were used as signal labels for target cytokines for performing a sandwich immunoassay (**Figure 1B**). In this strategy, each target cytokine molecule captured by the sensing CAb will be labeled with one AuNP. This formed immunocomplexes (CAb-cytokine-DAb-AuNP) will exhibit a light-scattering nanoplasmonic signal from the carried AuNPs due to the coupling phenomenon of LSPR (Gao, Song et al. 2021). The light-scattering nanoplasmonic signal can be captured by a darkfield optical microscope, allowing digital detection of cytokines at a single particle level with superior sensitivity and specificity.

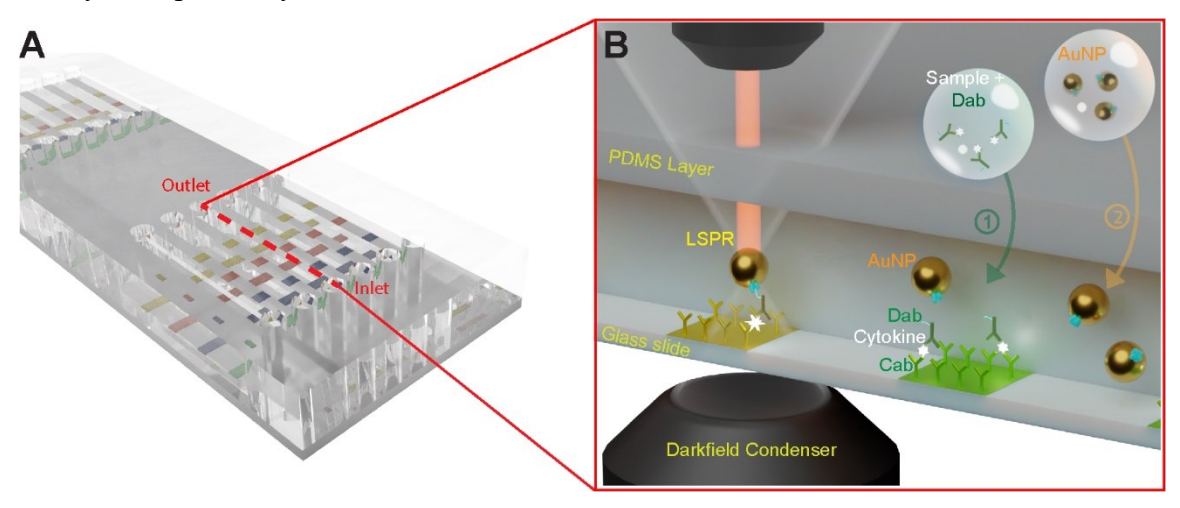


Figure 1. A microfluidic nanoplasmonic microarray immunosensor for multiplex cytokine detection. (A) A schematic showing the design of the microfluidic nanoplasmonic microarray immunosensor. (B) Principle of the nanoplasmonic immunosensor. Cytokine molecules form sandwich structure on immobilized CAbs with DAbs, which are then labeled by AuNPs with intense nanoplasmonic scattering signal.

This microarray chip was fabricated with a PDMS slab containing 12 parallel microfluidic channels reversibly bonded to a standard microscope glass slide (**Figure 2A, top**), following a microfluidic flow-patterning procedure (Chen, Chung et al. 2015, Gao, Song et al. 2021). Each

channel has dimensions of 500 µm (width) × 50 µm (height) × 63 mm (length). After the microfluidic patterning channel layer was first temporarily bond to the glass substrate, functionalization chemicals including APTES, glutaraldehyde, and CAb solutions were sequentially loaded into each patterning channel to immobilize CAb molecules onto the glass slide and form the multi-CAb strips for cytokine capture (**Figure 2B**). We confirmed the successful immobilization of CAbs onto glass substrates by mixing fluorophore-conjugated control antibody in the CAb solution, and observing the presence of the fluorescent signal on the CAb stride (**Figure 2C**). Furthermore, we measured the topography of the glass substrate with CAb strides using atomic force microscope (AFM), and observed altered topography and increased roughness on the CAb-functionalized surface compared with glass substrate outside the CAb stride (**Figure 2D**).

After the fabrication of multi-CAb strips, we then replaced the PDMS patterning channel layer from the glass substrate with a PDMS slab containing parallel sample-flow channels (Figure **2A, bottom**) orthogonal to the multi-CAb strips for sample loading and washing. Each microfluidic sample-flow channel has dimensions of 500 µm (width), 50 µm (height), 18 mm (length) and the inlet and outlet have a diameter of 1 mm, which minimize the required sample volume for each detection in each microfluidic channel to only 5-6 μL. In parallel with the multi-CAb strip fabrication, we prepared streptavidin-conjugated AuNPs through the EDC/NHS chemistry (Gao, Ye et al. 2020) on AuNPs with lipoic acid coating for later cytokine labeling. Testing samples were mixed with the DAb, and then loaded onto the CAb sensing strips through the microfluidic sample-flow channels using a micropipette. After 1-hour incubation, each target cytokine molecule was captured by the sensing CAb, labeled with DAb-AuNP forming sandwich structure on the chip. We confirmed the immune complex formation with a scanning electron microscope measurement on a silicon substrate, and observed immobilized AuNPs on the substrate (Figure 2E). Upon target analyte binding to AuNP, the unique LSPR coupling resulted in a bright plasmonic light-scattering signal from each AuNP, which can be captured using a darkfield LSPR imaging technique (Chen, Chung et al. 2015). The intense scattering of the immobilized AuNPs showed bright dots under darkfield microscopy (Figure 2F), and the number of bright dots in each sensing area was correlated with the concentration of the cytokine (Figure 2G). Together, the nanopasmonic immunosensor chip featured multiplexed detection of cytokines from multiple samples, where each intersection of a CAb strip and a sample loading channel formed an effective

detection area, with 12 CAb strips for 6 target cytokines (2 repeats for each cytokine) and 10 sample-flow channels to form 120 spots on a single chip (**Figure 2F**).

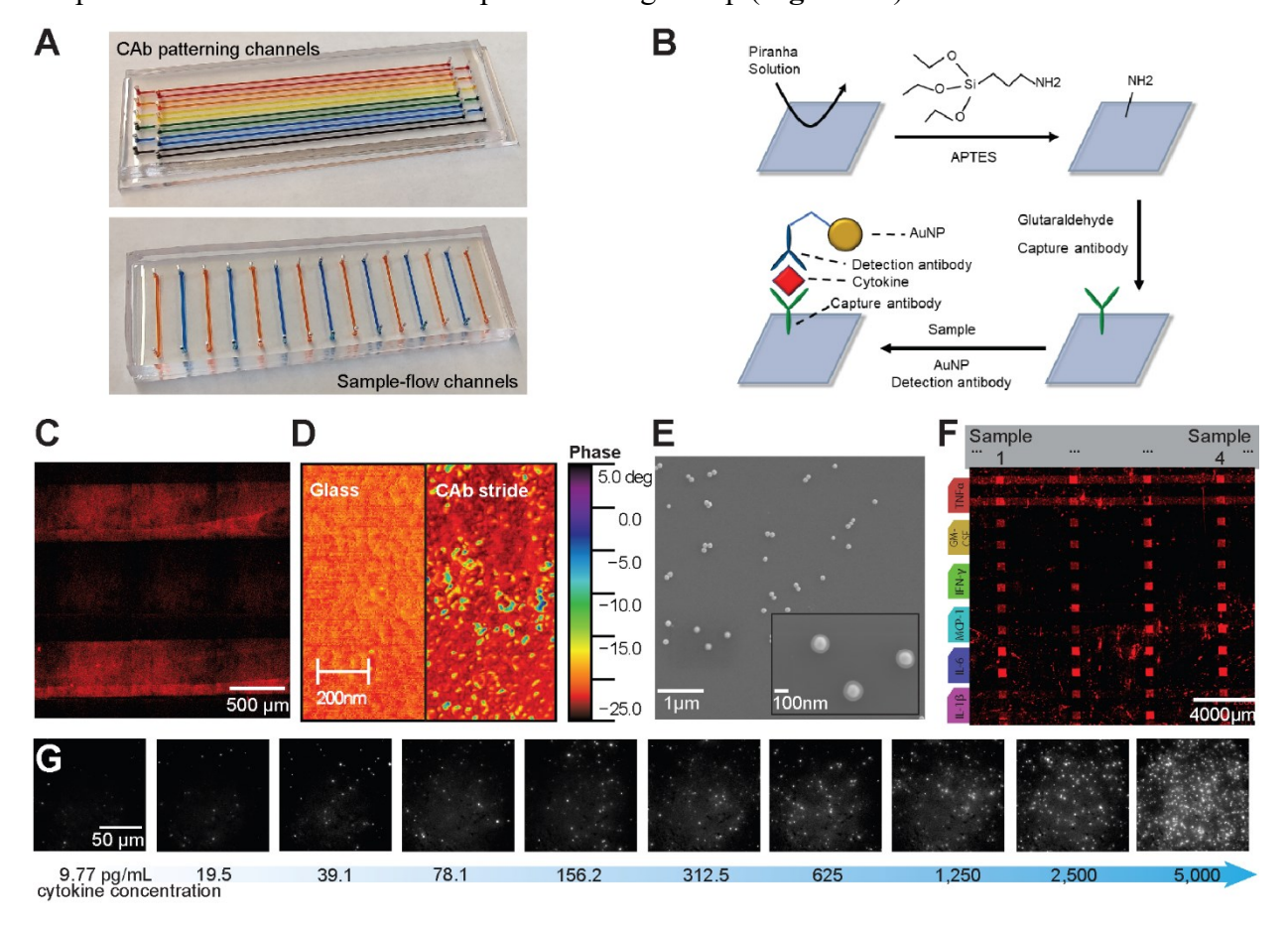


Figure 2. Characterization of the nanoplasmonic microarray immunosensor. (A) Photos of the chip with temporarily bond microfluidic CAb patterning channels (top) and sample-flow channels (bottom). These channels were filled with substituting water with food dyes (AmriColor). (B) A scheme of the chip preparation and cytokine detection method. (C) APC-labeled mouse IgG1 was mixed with CAb to demonstrate the formation of CAb strips on glass substrate. (D) AFM images showing areas outside ('glass') and inside ('CAb stride') the CAb stride of a microarray. The surface topography and roughness of the CAb stride showed difference from the glass area, due to immobilization of CAbs. (E) SEM image showing AuNPs immobilized on a silicon substrate through the same immune complex formation process as our microarray. Silicon substrate was chosen so coating was not needed. (F) A representative image showing a nanoplasmonic microarray with detection sites formed on the glass substrate. (G) The intense scattering from the AuNPs shows bright dots under darkfield microscopy, and the number of bright dots in each detection site is correlated with the concentration of the cytokine.

# 3.2. Precise measurement using digital readout

To quantify the analyte binding events, traditional methods for LSPR use the overall brightness of plasmonic light-scattering signals from all the nanoparticles in the sensing area (Chen, Huang et

al. 2015). Such an analog signal (**Figure 3A**) has limitations, for example, the accuracy would be negatively impacted by the non-uniformity of the brightness of the nanoparticles, the background noise, and the fluctuation of illumination in an optical system. Herein, we developed a digital imaging analysis method (**Figure 3B**), where the number of the immobilized AuNPs on the sensing surface were digitally readout based on the plasmonic scattering light upon each cytokine molecule-AuNP binding and converted to the concentration of cytokine, which presumably fits in a linear equation or a Logistic equation if saturation was observed.

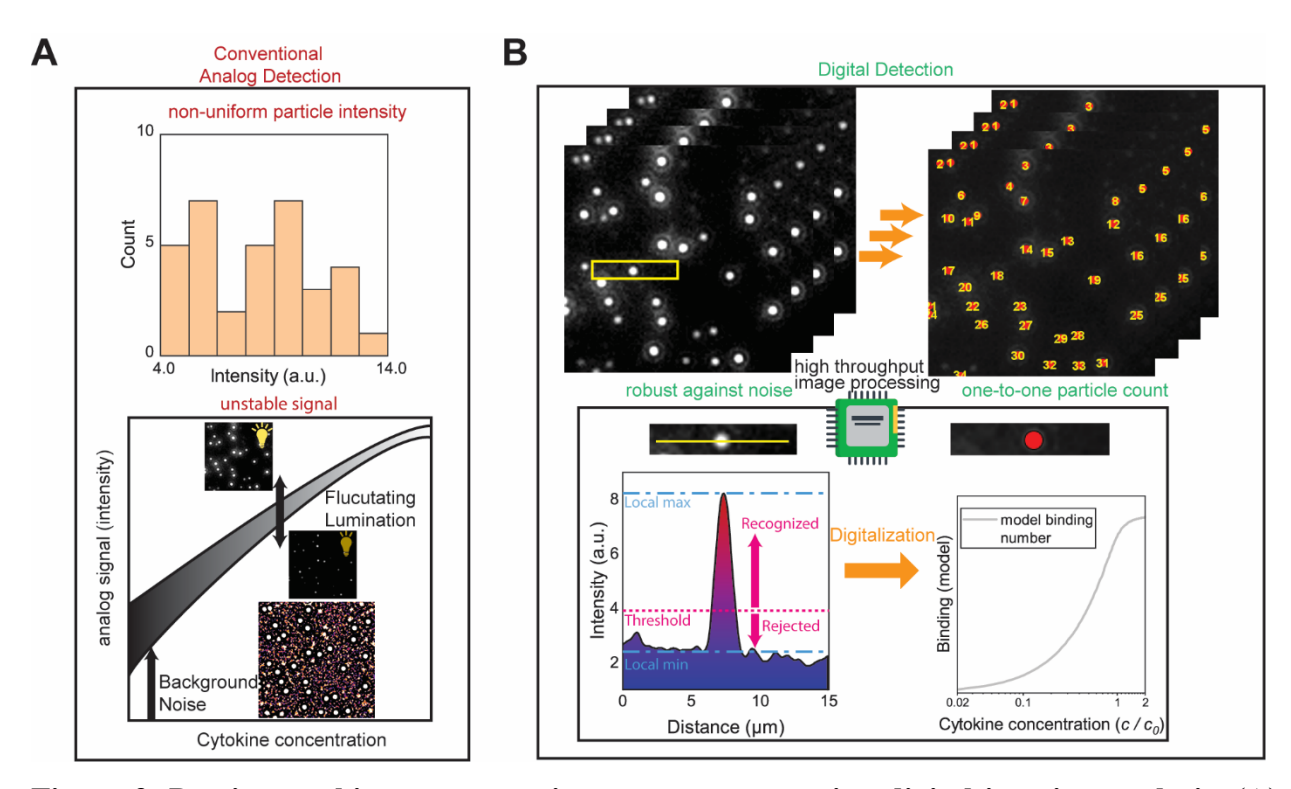
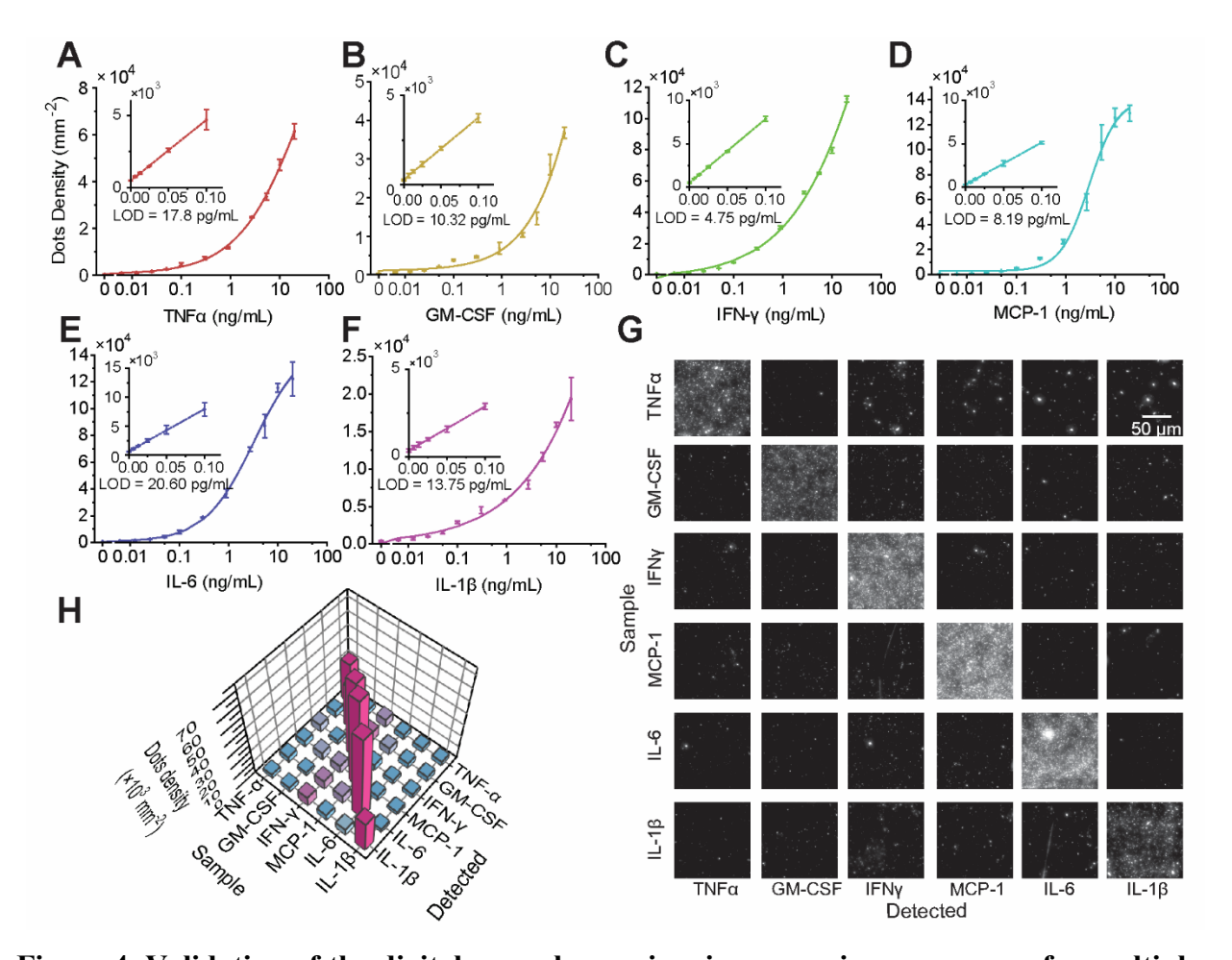


Figure 3. Precise cytokine concentration measurement using digital imaging analysis. (A) Conventional analog detection using the intensity of the scattered light is prone to non-uniformity in particle intensity, fluctuation in illumination, and background noise, adding to error of cytokine concentration measurement. (B) A digital imaging analysis using local maxima recognition extracts bright dots of particle scattering from the background and is robust against noise.

We evaluated the performance of the digital nanoplasmonic microarray immunosensor using a group of serum samples spiked with of cytokine standards at various concentrations (0-20,000 pg/mL). We first established calibration curves of 6 different cytokines (TNF-α, IFN-γ, MCP-1, GM-CSF, IL-1β, and IL-6) by plotting the numbers of the immobilized AuNPs against the concentrations of testing cytokines (**Figure 4A-F**) and calculated the sensitivity and dynamic range of the sensor. The results demonstrated that our digital nanoplasmonic immunosensor

achieved an ultra-sensitive detection of cytokines with limit of detection (LOD) down to 4.75-35.42 pg/mL in an extremely wide dynamic range (10-10<sup>4</sup> pg/mL). One of the most significant challenges associated with multiplex immunoassays is the crosstalk between the DAbs and CAbs for different analytes that may lead to noise or fake signals (Chen, Huang et al. 2015). Therefore, we checked the specificity of our multiplexed immunoassay towards each cytokine by cross-checking cytokine samples on the array of CAbs of other cytokines. The results showed negligible crosstalk during detection of these cytokines (**Figure 4G-H**), which validated that our immunoassay can be used for multiplex detection of various cytokines from the same biological sample.



**Figure 4. Validation of the digital nanoplasmonic microarray immunosensor for multiplex cytokine detection.** (A-F) Calibration curves of concentrations of six cytokines to the number of bright spots per detection area of immobilized AuNPs. Error bars denote mean ± standard deviation (SD). (G-H) Multiplex detection of six cytokines (5 ng/mL), i.e., TNF-α, GM-CSF, IFN-γ, MCP-1, IL-6, and IL-1β, demonstrated negligible crosstalk between six cytokines on each detection site.

# 3.3. In vitro monitoring of cytokine secretion dynamics during B-ALL CAR T-cell therapy with a Leukemia-on-a-Chip model.

We adapted a microfluidic in vitro human Leukemia-on-a-Chip B-ALL bone marrow niche model (Ma, Witkowski et al. 2020) to study cytokine secretions during CAR T-cell therapy (**Figure 5**). The Leukemia-on-a-Chip was a compartmentalized chip, where HUVEC and B-ALL leukemia cell line (Reh) were loaded into the inner ring region, and macrophages derived from THP-1 cell line and human lung fibroblasts were infused into the outer ring, respectively in a 3D fibrin gel. We added macrophages to monitor the immune response contributed by tissue-resident macrophages, which was recently found to be an important promotor for CRS (Giavridis, van der Stegen et al. 2018). The Leukemia-on-a-Chip model was cultured for 5 days, during which HUVEC formed vasculature representing the capillaries and B-ALL distributed among the vessel networks (Figure 5A), forming a 3D biomimetic B-ALL bone marrow niche. Following this, anti-CD19 4-1BB\delta CAR T-cells at three different dosages (0, 5k, and 25k) were loaded from the central hole into the vasculature networks (Figure 5B). The results showed that CAR T-cells eliminated B-ALL cells in a dose-dependent manner (Figure 5C), resembling the progress of B-ALL and the CAR T-cell therapy effects. As observed, high CAR T-cell dosage (25k) achieved the best cell killing effect, while low CAR T-cell dosages (5k) largely inhibited the leukemia cell growth but could not achieve remission over 5-day monitoring.

We next utilized our digital nanoplasmonic microarray immunosensor to monitor the release of 6 key cytokines (TNF-α, IFN-γ, MCP-1, GM-CSF, IL-1β, and IL-6) which are related to inflammation responses and T-cell killing effect (Singh, Anshita et al. 2021, Balagopal, Sasaki et al. 2022) from the *in vitro* human Leukemia-on-a-Chip bone marrow niche model during on-chip CAR T-cell treatment (**Figure 5D&E, Figure S1**). To dynamically monitor the performance of CAR T-cell treatment on-chip, cell culture media were sampled from the devices treated with different CAR T-cell dosages every 24 hours from day 0 to day 5. Following this, CAR T-cell culture media samples were then loaded to the nanoplasmonic microarray to measure how many cytokines were secreted in the B-ALL bone marrow niche each day. As a result, we observed a heterogenous profile of cytokine secretion dynamics of different cytokines from the B-ALL bone marrow niche at different treatment conditions. Among those 6 cytokines, IL-6 and MCP-1 secretion (**Figure 5D&E, Figure S1**) showed significant higher concentrations and dramatic

changes during CAR T-cell therapy. Interestingly, both IL-6 and MCP-1 reached a peak secretion on day 2 and then gradually declined on days 3 and 4 from high CAR T-cell dosage (25k) group, while the peaks of IL-6 and MCP-1 from low CAR T-cell dosage (5k) group delayed to day 4 (**Figure 5E, Figure S1**). Such a dynamic secretion of IL-6 and MCP-1 correlated with the effector-to-target (CAR T-cell to leukemia burden), where high dosage of CAR T-cells achieved a strong killing of B-ALL cells and thus rapidly induced immune response from the leukemia microenvironment, as compared to that from low dosage of CAR T-cells.

The other 4 cytokines, TNF-α, IL-1β, IFN-γ and GM-CSF, were detected at low levels (**Figure 5E, Figure S1**). It was reported that MCP-1 releasing is related to IFN-γ (Han, Li et al. 2012) whereas MCP-1 and IL-6 releasing is largely correlated TNF-α (Mueller, von Seggern et al. 2010). Therefore, IFN-γ and TNF-α may function in a low level of concentration. GM-CSF is mainly secreted by macrophage while THP-1 derived macrophage may not express it (Chanput, Mes et al. 2014), and by replacing the cell line, we may see more secretion of GM-CSF. IL-1β mainly results from pathogen associated molecular patterns (PAMP) (Brough, Tyrrell et al. 2011), which is associated with immune reactions against infections not relevant to our CAR T-cell system. Together, our findings agreed with the current explanation for the start of a CRS during CAR T-cell therapy (Hao, Li et al. 2020, Liu, Fang et al. 2020), where IL-6 is considered as the gold standard for CRS monitoring (Porter, Frey et al. 2018). CAR T-cell therapy inflicts a positive feedback release of pro-inflammatory cytokines, during which effector molecules such as Gasdermin E can activate macrophages to release more pro-inflammatory cytokines such as IL-6 and MCP-1 (Deshmane, Kremlev et al. 2009, Tanaka, Narazaki et al. 2016, Wang and Han 2018, Singh, Anshita et al. 2021).

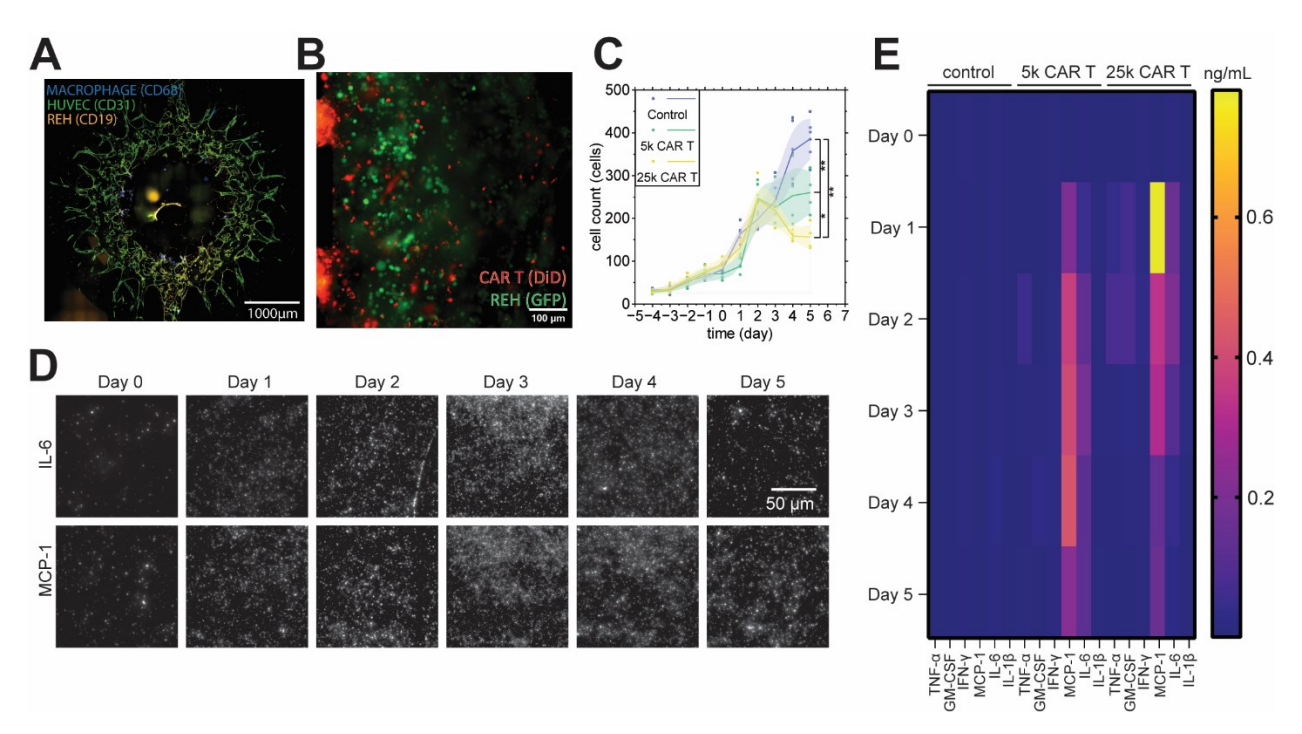


Figure 5. Leukemia-on-a-chip system and cytokine detection using the digital nanoplasmonic microarray immunosensor. (A) Fluorescent image of the engineered leukemia bone marrow niche with HUVEC vascular network (CD31 in green), Reh leukemia cells (CD19 in yellow), and macrophages (CD68 in Cyan). (B) Fluorescent image of CAR T-cell (DiD, red) infusion into the leukemia niche (GFP, green). (C) Quantifications of leukemia burdens on-chip treated with CAR T-cells (5k and 25k) or left untreated. In the figure, each point represents a count of live leukemia cells from individual 20x field view image. The line represents the average count of leukemia blasts from four images collected from two devices and the band represents the error bar for each condition. Statistical analysis was performed using Tukey test on one-way analysis of variance (ANOVA). \*p <0.05, \*\*p<0.01. (D) Darkfield microscopy images of immobilized AuNPs for detection of II-6 and MCP-1 from day 0 to day 5. (E) Cytokine concentration graph of the selected 6 cytokines measured from day 0 to day 5. All data were averaged from three independent experiments. The detailed concentrations are shown in supporting Figure S1.

# 4. Conclusions

New multiplexed assays that can profile a matrix of cytokines rapidly, with high-throughput, using small amounts of a sample are in an urgent need for monitoring the disease progression and providing new insights for improving cancer immunotherapies. Previously, we developed a nanoplasmonic sandwich immunoassay to characterize tumor-derived exosome and profile exosomal PD-L1 expression using LSPR-based label-free quantitative analysis (Wang, Huang et al. 2021). Following this, we developed a microfluidic nanoplasmonic digital immunoassay for profiling cytokine storm in COVID-19 patients using machine-learning-assisted image analysis

(Gao, Song et al. 2021). To broaden the application of our biosensing approach for implementation on highly functional biochip system such as organ-on-a-chip, we herein established a digital nanoplasmonic microarray immunosensor to monitor cytokine secretions from a Leukemia-on-a-Chip B-ALL bone marrow niche model under CAR T-cell therapy. Using this novel digital nanoplasmonic biosensing approach, we were able to detect six cytokines with neglectable cross talk in a rapid, sensitive, and high-multiplex manner. As a proof-of-concept, we successfully applied our digital nanoplasmonic immunosensor for a comprehensive and temporal profiling of the six key cytokines from the leukemia microenvironment during CAR T-cell therapy, which conventional ELISA methods cannot achieve. Most importantly, our digital nanoplasmonic microarray immunosensor requires only a small volume of sample while allows for the test of a broader range of cytokines, which can be easily adopted for continuously monitoring systematic immune responses (Vidal, Kawabata et al. 2010). CRS is a systematic response of patients reacts to CAR T-cell therapy, which involve multiple tissues and organs such as bone marrow where the disease is initiated. Measurement of cytokines secreted each day in the B-ALL bone marrow niche during the on-chip CAR T-cell treatment from such a biomimetic human CAR T-cell therapy modeling system allow us to study systematic immune response and interactions between CAR Tcells, leukemia, and the bone marrow immune microenvironment, and potentially predict the possibility of developing a CRS in patient treated with CAR T-cell therapy. We envision that functional integration of our biosensing approach with a multi-organ chip system populated with patient-derived samples may help to monitor systematic responses associated with CRS during CAR T-cell therapy as well as other virus-related infectious diseases such as COVID-19 (Azar, Shin et al. 2020, Herland, Maoz et al. 2020, Hong, Ahn et al. 2020, Santoso, Li et al. 2020, Que, Hu et al. 2022).

#### **CRediT** authorship contribution statement

Benteng Ma: Conceptualization, Methodology, Investigation, Formal analysis, Visualization, and, Writing – original draft. Xinya Liu: Investigation, Formal analysis, Data curation. Zhuoyu Zhang: Methodology, Investigation, Formal analysis, and, Writing – original draft. Chao Ma: Conceptualization, Writing – review & editing. Rashik Chand: Investigation. Saee Patwardhan: Investigation. Chuanyu Wang: Methodology, Writing – review & editing. Soracha D. Thamphiwatana: Conceptualization, Supervision, Writing – review & editing. Pengyu Chen: Conceptualization, Supervision, Writing – review & editing. Weiqiang Chen: Conceptualization, Supervision, Writing – review & editing.

# **Declaration of competing interest**

The authors declare that they have no known competing financial interests or personal relationships that could have appeared to influence the work reported in this paper.

#### Acknowledgements

This work was supported by the National Science Foundation (CBET-2103219 and CBET-1943302), the US National Institutes of Health (R35GM133646 and R35GM133795), the Cancer Research Institute Irvington Postdoctoral Fellowship (CRI4018), the Scholarship for Short-term Visiting Scholars at Mahidol University.

# Data availability

Data will be made available on request.

# References

- Alizadeh, D., R. A. Wong, S. Gholamin, M. Maker, M. Aftabizadeh, X. Yang, J. R. Pecoraro, J. D. Jeppson, D. Wang, B. Aguilar, R. Starr, C. B. Larmonier, N. Larmonier, M. H. Chen, X. Wu, A. Ribas, B. Badie, S. J. Forman and C. E. Brown (2021). "IFNgamma Is Critical for CAR T Cell-Mediated Myeloid Activation and Induction of Endogenous Immunity." <u>Cancer Discov</u> **11**(9): 2248-2265.
- Aydin, S. (2015). "A short history, principles, and types of ELISA, and our laboratory experience with peptide/protein analyses using ELISA." <u>Peptides</u> **72**: 4-15.
- Azar, M. M., J. J. Shin, I. Kang and M. Landry (2020). "Diagnosis of SARS-CoV-2 infection in the setting of the cytokine release syndrome." <u>Expert Rev Mol Diagn</u> **20**(11): 1087-1097.
- Balagopal, S., K. Sasaki, P. Kaur, M. Nikolaidi and J. Ishihara (2022). "Emerging approaches for preventing cytokine release syndrome in CAR-T cell therapy." <u>J Mater Chem B</u> **10**(37): 7491-7511.
- Bonifant, C. L., H. J. Jackson, R. J. Brentjens and K. J. Curran (2016). "Toxicity and management in CAR T-cell therapy." <u>Mol Ther Oncolytics</u> **3**: 16011.
- Brough, D., P. J. Tyrrell and S. M. Allan (2011). "Regulation of interleukin-1 in acute brain injury." <u>Trends Pharmacol Sci</u> **32**(10): 617-622.
- Brudno, J. N. and J. N. Kochenderfer (2019). "Recent advances in CAR T-cell toxicity: Mechanisms, manifestations and management." <u>Blood Rev</u> **34**: 45-55.
- Chanput, W., J. J. Mes and H. J. Wichers (2014). "THP-1 cell line: an in vitro cell model for immune modulation approach." <u>Int Immunopharmacol</u> **23**(1): 37-45.
- Chen, P., N. T. Huang, M. T. Chung, T. T. Cornell and K. Kurabayashi (2015). "Label-free cytokine micro- and nano-biosensing towards personalized medicine of systemic inflammatory disorders." Adv Drug Deliv Rev **95**: 90-103.
- Chen, P. Y., M. T. Chung, W. McHugh, R. Nidetz, Y. W. Li, J. P. Fu, T. T. Cornell, T. P. Shanley and K. Kurabayashi (2015). "Multiplex Serum Cytokine Immunoassay Using Nanoplasmonic Biosensor Microarrays." <u>Acs Nano</u> **9**(4): 4173-4181.
- Deshmane, S. L., S. Kremlev, S. Amini and B. E. Sawaya (2009). "Monocyte chemoattractant protein-1 (MCP-1): an overview." <u>J Interferon Cytokine Res</u> **29**(6): 313-326.
- Freer, G. and L. Rindi (2013). "Intracellular cytokine detection by fluorescence-activated flow cytometry: basic principles and recent advances." <u>Methods</u> **61**(1): 30-38.
- Gao, Z., Y. Song, T. Y. Hsiao, J. He, C. Wang, J. Shen, A. MacLachlan, S. Dai, B. H. Singer, K. Kurabayashi and P. Chen (2021). "Machine-Learning-Assisted Microfluidic Nanoplasmonic Digital Immunoassay for Cytokine Storm Profiling in COVID-19 Patients." <u>ACS Nano</u>.
- Gao, Z., H. Ye, Q. Wang, M. J. Kim, D. Tang, Z. Xi, Z. Wei, S. Shao and X. Xia (2020). "Template Regeneration in Galvanic Replacement: A Route to Highly Diverse Hollow Nanostructures." <u>ACS Nano</u> **14**(1): 791-801.
- Giavridis, T., S. J. C. van der Stegen, J. Eyquem, M. Hamieh, A. Piersigilli and M. Sadelain (2018). "CAR T cell-induced cytokine release syndrome is mediated by macrophages and abated by IL-1 blockade." <u>Nat Med</u> **24**(6): 731-738.
- Han, Y. L., Y. L. Li, L. X. Jia, J. Z. Cheng, Y. F. Qi, H. J. Zhang and J. Du (2012). "Reciprocal interaction between macrophages and T cells stimulates IFN-gamma and MCP-1 production in Ang II-induced cardiac inflammation and fibrosis." <u>PLoS One</u> 7(5): e35506.
- Hao, Z., R. Li, L. Meng, Z. Han and Z. Hong (2020). "Macrophage, the potential key mediator in CAR-T related CRS." Exp Hematol Oncol 9: 15.

- Herland, A., B. M. Maoz, D. Das, M. R. Somayaji, R. Prantil-Baun, R. Novak, M. Cronce, T. Huffstater, S. S. F. Jeanty, M. Ingram, A. Chalkiadaki, D. Benson Chou, S. Marquez, A. Delahanty, S. Jalili-Firoozinezhad, Y. Milton, A. Sontheimer-Phelps, B. Swenor, O. Levy, K. K. Parker, A. Przekwas and D. E. Ingber (2020). "Quantitative prediction of human pharmacokinetic responses to drugs via fluidically coupled vascularized organ chips." <u>Nat Biomed Eng</u> 4(4): 421-436.
- Hong, K. S., J. H. Ahn, J. G. Jang, J. H. Lee, H. N. Kim, D. Kim and W. Lee (2020). "GSK-LSD1, an LSD1 inhibitor, quashes SARS-CoV-2-triggered cytokine release syndrome in-vitro." Signal Transduct Target Ther 5(1): 267.
- Lim, H. J., T. Saha, B. T. Tey, W. S. Tan and C. W. Ooi (2020). "Quartz crystal microbalance-based biosensors as rapid diagnostic devices for infectious diseases." <u>Biosens Bioelectron</u> **168**: 112513.
- Liu, Y., Y. Fang, X. Chen, Z. Wang, X. Liang, T. Zhang, M. Liu, N. Zhou, J. Lv, K. Tang, J. Xie, Y. Gao, F. Cheng, Y. Zhou, Z. Zhang, Y. Hu, X. Zhang, Q. Gao, Y. Zhang and B. Huang (2020). "Gasdermin E-mediated target cell pyroptosis by CAR T cells triggers cytokine release syndrome." <u>Sci Immunol</u> **5**(43).
- Ma, C., M. T. Witkowski, J. Harris, I. Dolgalev, S. Sreeram, W. Qian, J. Tong, X. Chen, I. Aifantis and W. Chen (2020). "Leukemia-on-a-chip: Dissecting the chemoresistance mechanisms in B cell acute lymphoblastic leukemia bone marrow niche." <u>Sci Adv</u> 6(44).
- Mayer, K. M. and J. H. Hafner (2011). "Localized surface plasmon resonance sensors." <u>Chem Rev</u> **111**(6): 3828-3857.
- Mora, J., A. Given Chunyk, M. Dysinger, S. Purushothama, C. Ricks, K. Osterlund and V. Theobald (2014). "Next generation ligand binding assays-review of emerging technologies' capabilities to enhance throughput and multiplexing." <u>AAPS J</u> 16(6): 1175-1184.
- Mueller, L., L. von Seggern, J. Schumacher, F. Goumas, C. Wilms, F. Braun and D. C. Broering (2010). "TNF-alpha similarly induces IL-6 and MCP-1 in fibroblasts from colorectal liver metastases and normal liver fibroblasts." <u>Biochem Biophys Res Commun</u> **397**(3): 586-591.
- Porter, D., N. Frey, P. A. Wood, Y. Weng and S. A. Grupp (2018). "Grading of cytokine release syndrome associated with the CAR T cell therapy tisagenlecleucel." <u>J Hematol Oncol</u> **11**(1): 35.
- Prussin, C. and D. D. Metcalfe (1995). "Detection of intracytoplasmic cytokine using flow cytometry and directly conjugated anti-cytokine antibodies." <u>Journal of Immunological Methods</u> **188**(1): 117-128.
- Que, Y., C. Hu, K. Wan, P. Hu, R. Wang, J. Luo, T. Li, R. Ping, Q. Hu, Y. Sun, X. Wu, L. Tu, Y. Du, C. Chang and G. Xu (2022). "Cytokine release syndrome in COVID-19: a major mechanism of morbidity and mortality." <u>Int Rev Immunol</u> **41**(2): 217-230.
  - Sadelain, M. (2017). "CD19 CAR T Cells." Cell 171(7): 1471.
- Santoso, C. S., Z. Li, J. T. Rottenberg, X. Liu, V. X. Shen and J. I. F. Bass (2020). "In vitro Targeting of Transcription Factors to Control the Cytokine Release Syndrome in COVID-19." bioRxiv.
- Singh, S., D. Anshita and V. Ravichandiran (2021). "MCP-1: Function, regulation, and involvement in disease." <u>Int Immunopharmacol</u> **101**(Pt B): 107598.
- Song, Y., E. Sandford, Y. Tian, Q. Yin, A. G. Kozminski, S. H. Su, T. Cai, Y. Ye, M. T. Chung, R. Lindstrom, A. Goicochea, J. Barabas, M. Olesnavich, M. Rozwadowski, Y. Li, H. B. Alam, B. H. Singer, M. Ghosh, S. W. Choi, M. Tewari and K. Kurabayashi (2021). "Rapid single-molecule digital detection of protein biomarkers for continuous monitoring of systemic immune disorders." <u>Blood</u> **137**(12): 1591-1602.

- Taguchi, T., J. R. McGhee, R. L. Coffman, K. W. Beagley, J. H. Eldridge, K. Takatsu and H. Kiyono (1990). "Detection of individual mouse splenic T cells producing IFN-γ and IL-5 using the enzyme-linked immunospot (ELISPOT) assay." <u>Journal of Immunological Methods</u> **128**(1): 65-73.
- Tanaka, T., M. Narazaki and T. Kishimoto (2016). "Immunotherapeutic implications of IL-6 blockade for cytokine storm." Immunotherapy **8**(8): 959-970.
- Vidal, J. M., T. T. Kawabata, R. Thorpe, B. Silva-Lima, K. Cederbrant, S. Poole, J. Mueller-Berghaus, M. Pallardy and J. W. Van der Laan (2010). "In vitro cytokine release assays for predicting cytokine release syndrome: the current state-of-the-science. Report of a European Medicines Agency Workshop." <a href="Cytokine">Cytokine</a> 51(2): 213-215.
- Vignali, D. A. A. (2000). "Multiplexed particle-based flow cytometric assays." <u>Journal of Immunological Methods</u> **243**(1-2): 243-255.
- Wang, C., C. H. Huang, Z. Gao, J. Shen, J. He, A. MacLachlan, C. Ma, Y. Chang, W. Yang, Y. Cai, Y. Lou, S. Dai, W. Chen, F. Li and P. Chen (2021). "Nanoplasmonic Sandwich Immunoassay for Tumor-Derived Exosome Detection and Exosomal PD-L1 Profiling." <u>ACS Sens</u> **6**(9): 3308-3319.
- Wang, Z. and W. Han (2018). "Biomarkers of cytokine release syndrome and neurotoxicity related to CAR-T cell therapy." Biomark Res **6**: 4.
- Wang, Z., Z. Wu, Y. Liu and W. Han (2017). "New development in CAR-T cell therapy." <u>J Hematol Oncol</u> **10**(1): 53.
- Witkowski, M. T., I. Dolgalev, N. A. Evensen, C. Ma, T. Chambers, K. G. Roberts, S. Sreeram, Y. Dai, A. N. Tikhonova, A. Lasry, C. Qu, D. Pei, C. Cheng, G. A. Robbins, J. Pierro, S. Selvaraj, V. Mezzano, M. Daves, P. J. Lupo, M. E. Scheurer, C. A. Loomis, C. G. Mullighan, W. Chen, K. R. Rabin, A. Tsirigos, W. L. Carroll and I. Aifantis (2020). "Extensive Remodeling of the Immune Microenvironment in B Cell Acute Lymphoblastic Leukemia." <u>Cancer Cell</u> **37**(6): 867-882 e812.